February 28, 2008

$d\sigma/dy$ distribution of Drell-Yan dielectron pairs

J. Han, A. Bodek
W. Sakumoto, Y. Chung

University of Rochester

(for the CDF Collaboration)

Abstract

We report on the measurement of the rapidity distribution, $d\sigma/dy$, over the full kinematic range for e^+e^- pairs in the Z boson region of $66 < M_{ee} < 116$ GeV/c^2. The data sample consists of 2.1 fb^{-1} of $p\bar{p}$ collisions at $\sqrt{s} = 1.96$ TeV taken by the Collider Detector at Fermilab. The $d\sigma/dy$ is compared with the NLO theory prediction.

1 Introduction

Measurement of the rapidity distribution and total cross section of Drell-Yan pairs from γ^*/Z production provide a stringent test of QCD calculations in leading order (LO) and next to leading order (NLO). Figure 1 shows the Feynman diagram for γ^*/Z boson production in the $p\bar{p}$ collision. In leading order, the process is $q + \bar{q} \to \gamma^*/Z$, i.e. a quark and anti-quark from the colliding hadron annihilates to form a virtual γ^*/Z boson. Two partons, carrying momentum fractions x_1 and x_2, participate in the interaction. The final state from this process is two leptons from the γ^*/Z decays. The emission of gluons in the initial state is taken into account in calculations which include next to leading order(NLO) corrections in the strong interaction. In LO, the momentum fraction $x_1(x_2)$ carried by the partons from the proton(antiproton) is related to the rapidity (y) of the Z boson via the equation:

$$x_1 = M_Z e^{y} s^{-1/2} \quad , \; x_2 = M_Z e^{-y} s^{-1/2} \tag{1}$$

where s is the center of mass energy and M_z is the mass of γ^*/Z boson. Figure 2 shows $x_1(x_2)$ as a function of y at the tevatron, $\sqrt{s} = 1.96$ TeV.

In this analysis, the $d\sigma(\gamma^*/Z)/dy$ distribution is measured using dielectrons from γ^*/Z decays. This analysis includes e^+e^- pairs from the forward calorimeter region.

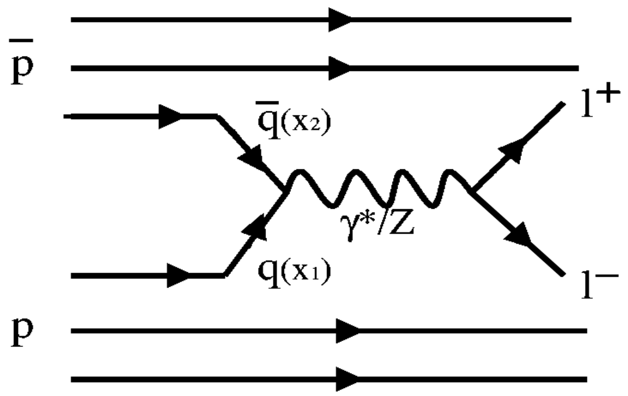

Figure 1: Feynman diagram of LO γ^*/Z production in a $p\bar{p}$ collision.

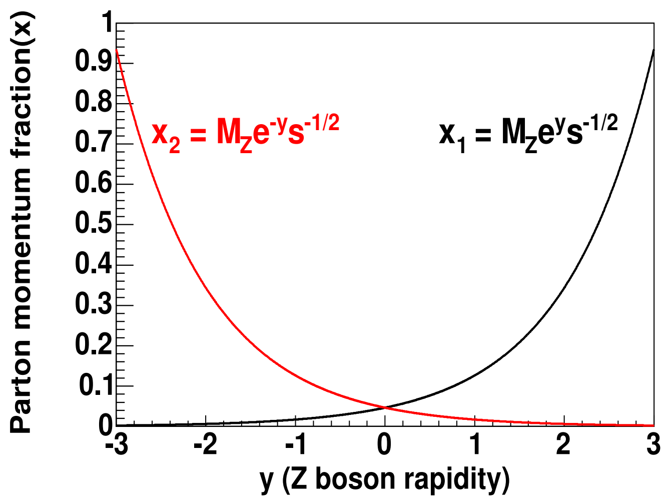

Figure 2: The relationship between the momentum fraction, x, and the rapidity of the γ^*/Z boson.

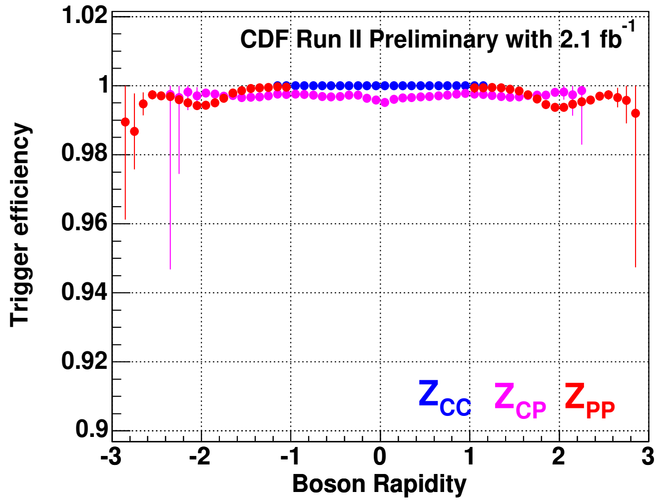

Figure 3: The trigger efficiencies versus dielectron pair rapidity. The blue dots give the efficiency for CC topology, the magenta dots give the efficiency for CP topology and the red dots give the efficiency for PP topology.

2 Data Sample and Event Selection

The data consists of 2.1 fb^{-1}. The events come from the inclusive single central electron or the dielectron trigger. The dielectron data sample consists of three different e^+e^- pair topologies. The CC topology has two electrons in the central calorimeter with $|\eta| < 1.1$. The CP topology has one electron in the central calorimeter with $|\eta| < 1.1$, and another in the plug calorimeter with $1.2 < |\eta| < 2.8$. The PP topology has two electrons in the plug calorimeter with $1.2 < |\eta| < 2.8$. In the CC and PP topology, we select electrons with $E_T \geq 25$ GeV. In the CP topology, we select electrons with $E_T \geq 20$ GeV. For all topologies, the $p\bar{p}$ collision vertex along the proton direction (z-axis) is required to be within 60 cm of the center of the detector.

The electron trigger efficiencies as a function of E_T are measured using the data. The individual electron trigger efficiencies are combined to form the overall trigger efficiency of dielectron pairs versus rapidity. The overall trigger efficiencies are almost 100%. Figure 3 shows the overall trigger efficiency for the CC, CP, and PP topologies.

For the CC topology, oppositely charged electron pairs are required. One electron has tight and another has loose central electron ID cuts [2]. For the CP topology, the central electron passes the tight central electron ID cuts and the plug electron passes the standard plug electron ID cuts [2]. For the PP topology, both electrons pass the standard plug electron ID cuts [2]. In addition, for the PP topology, the pseudo-rapidity must have the same sign, and at least one electron must have a silicon track to reduce the background. The Z rapidity of events with the PP topology reaches $|y| = 2.9$.

After the selection cuts, we find 50784 CC topology events, 85735 CP topology events, and 31259 PP topology events. Figure 4 shows the dielectron invariant mass and rapidity distributions for each topology.

3 Acceptance and Efficiency

Geometric and kinematic acceptances are modeled by using the PYTHIA $Z \rightarrow ee$ event generator combined with a GEANT simulation of the CDF detector. The simulation is tuned to data for the energy resolution and electron ID efficiency. Table 1 summarizes the total acceptance (A) and efficiency (ϵ) for each topology. Figure 5 shows the $A \times \epsilon$ as a function of the γ^*/Z boson rapidity. The $A \times \epsilon$ is flat up to $y \sim 2.0$ and is non-zero up to $|y| = 2.9$ with the PP topology.

Topology	Acceptance	Efficiency
CC	0.107 ± 0.001	$0.904 \pm 0.008(stat. + sys.)$
CP	0.231 ± 0.001	$0.701 \pm 0.003(stat. + sys.)$
PP	0.095 ± 0.001	$0.752 \pm 0.037(stat. + sys.)$

Table 1: Dielectron acceptances and efficiencies.

4 Silicon Tracking Efficiency

For the PP topology, one electron is required to be within the silicon fiducial range, and to have a silicon track associated with it. This track must have 3 or more silicon hits.

The track finding efficiency is measured using plug electrons from the PP topology in terms of the expected silicon layers which the electron can pass through and the number of ZVertices. The number of expected silicon layers is calculated using the electron η and the z location of the $p\bar{p}$ collision vertex ($z_{\rm vtx}$). There is a discrepancy in this efficiency between the data and MC. To account for this discrepancy in the MC, a scaling factor is applied. The scaling factor is the data to MC ratio of ϵ(expected slilcon layers, NVertices).

The scaled simulation is used to calculate the efficiency of the silicon track requirement in the PP topology as a function of the dielectron rapidity. It is shown in Figure 6. The tracking efficiency averaged over all PP dielectron rapidities is 0.864 ± 0.001.

5 Background Estimation

5.1 QCD Background

The main source of background in the analysis is QCD dijet background, which is estimated from the electron isolation energy distribution. The isolation energy, E_{iso}, is defined as the energy contained within a cone in (η, ϕ) of $\Delta R \leq 0.4$ around the electron minus the energy of the electron itself. The signal region is in the low E_{iso} region and the background is distributed over all E_{iso} but is dominant in the high E_{iso} region. To reduce the background, we apply the isolation cut, $E_{iso} \leq 4$ GeV. We fit the isolation distribution for both signal and background contributions and extrapolate

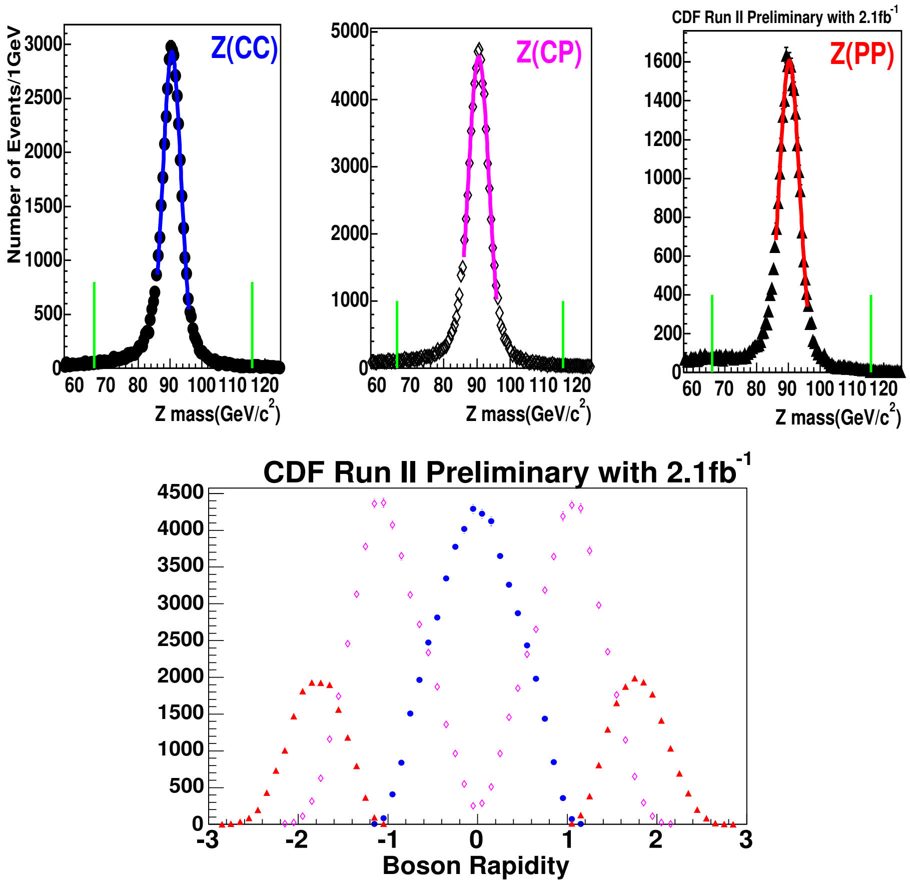

Figure 4: The top plots are the invariant mass distributions of the CC, CP and PP topology dielectrons. The lines show the mass limits of $d\sigma/dy(\gamma^*/Z)$ measurement, $66 < M_Z < 116 GeV/c^2$. The bottom plot shows the dielectron rapidity distribution. In the rapidity plot, the circles, diamonds, and triangles are the rapidities for the CC, CP, and PP topology dielectrons, respectively.

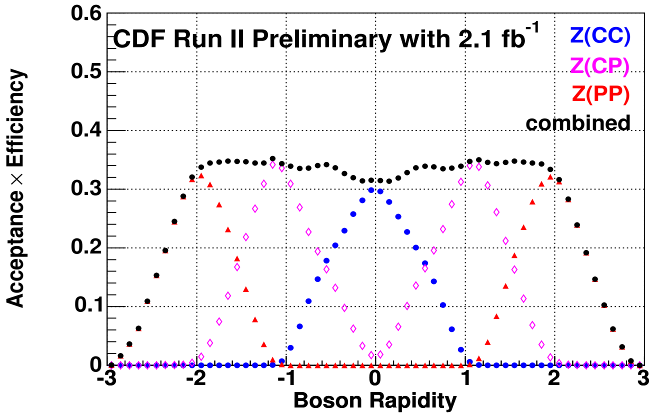

Figure 5: The product of the kinematic acceptance and the event selection efficiencies versus the dielectron rapidity. The circles, diamonds, and triangles are the rapidities for the CC, CP, and PP topology dielectrons, respectivly.

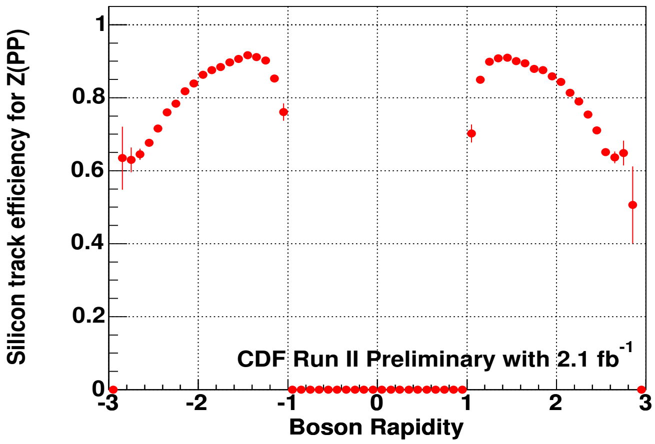

Figure 6: Efficiency of the silicon track requirement for the PP dielectron topology versus the dielectron rapidity.

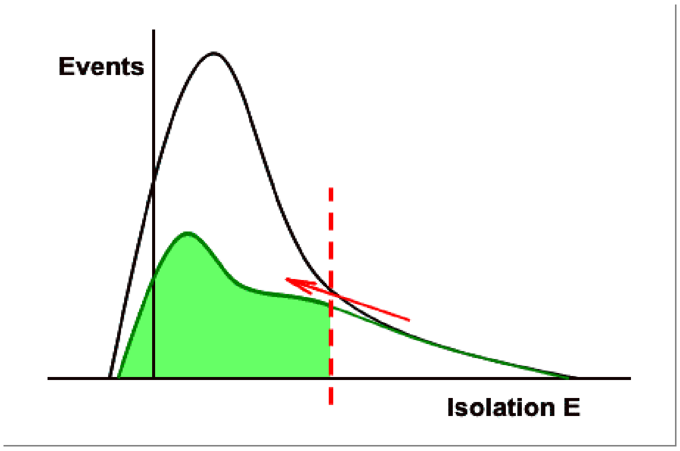

Figure 7: Cartoon of the background extrapolation into the signal region using the E_{iso} distribution. The upper curve is the overall E_{iso} distribution and the lower curve is the background E_{iso}.

the background from high isolation tail into the signal region of $E_{iso} \leq 4$ GeV. This background extrapolation is shown in the cartoon in Figure 7. The background is measured separately in each dielectron topology. The shape of the background E_{iso} distribution is measured using a background enriched sample. For the systematic uncertainty, we assign a 30% uncertainty for each topology. Table 2 summarizes the total background rates and uncertainties. The background shape versus the dielectron rapidity is obtained from the same background sample, and its overall normalization is set using the isolation extrapolation rate.

Topology	background rate (unit: %)
CC	$0.21 \pm 0.06(stat.) \pm 0.06(sys.)$
CP	$0.48 \pm 0.06(stat.) \pm 0.14(sys.)$
PP	$1.28 \pm 0.28(stat.) \pm 0.38(sys.)$

Table 2: The background rates and total systematic uncertainties.

5.2 Background from Electroweak and $t\bar{t}$ Processes

We measure the background rates and shapes from electroweak and $t\bar{t}$ processes using simulation. We consider four different processes and obtain the number of background events and the shape in the dielectron rapidity for each process. The backgrounds are summarized in Table 3.

6 Systematic Uncertainties

Systematic uncertainties are determined for:

	CC	CP	PP	Total
WW	20.0 ± 1.4	22.2 ± 1.6	3.3 ± 0.3	45.5 ± 2.1
WZ	34.8 ± 2.3	44.0 ± 3.0	12.5 ± 0.8	91.3 ± 3.9
$t\bar{t}$ inclusive	9.7 ± 0.7	6.6 ± 0.5	0.4 ± 0.1	16.7 ± 0.9
W inclusive	4.6 ± 2.1	25.6 ± 5.2	7.8 ± 2.7	38.0 ± 6.2

Table 3: The number of events and total systematic uncertainty from electroweak and $t\bar{t}$ processes in each dielectron topology.

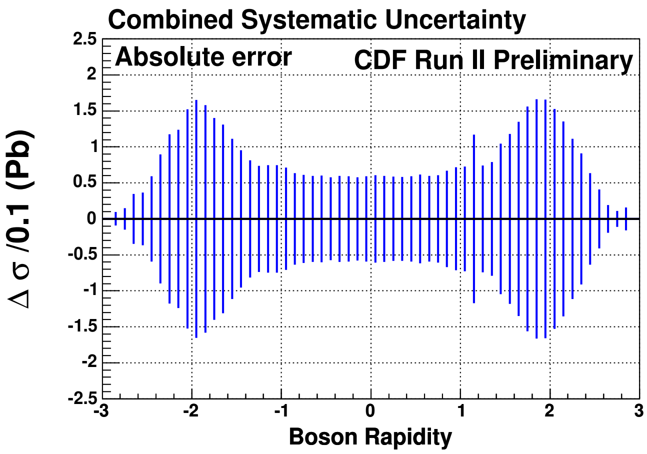

Figure 8: The total systematic uncertainties in the dielectron rapidity.

- Detector material modelling
- Background estimates
- Electron identification efficiencies
- Silicon tracking efficiency
- Acceptance
- Plug electron energy calibration

The largest systematic uncertainty is associated with the measurement of the electron identification efficiencies. Figure 8 shows the combined systematic uncertainty as a function of the dielectron rapidity.

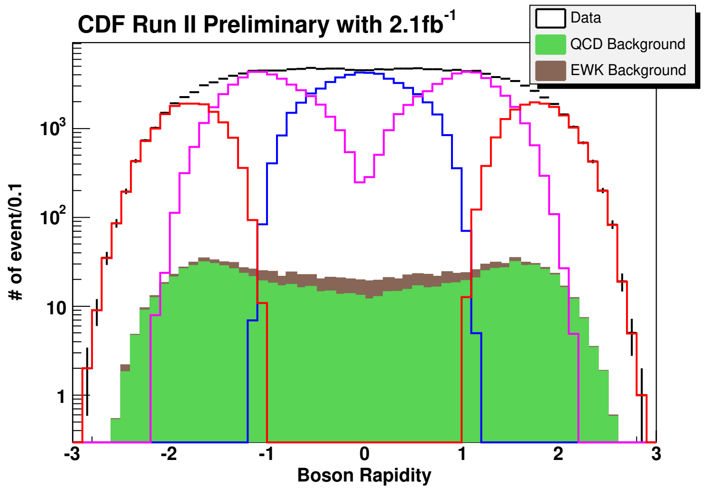

Figure 9: The dielectron rapidity distribution of the data and the backgrounds. Green histogram is the QCD background and brown histogram is the background from EWK process. Black line is all combined data events.

7 $d\sigma/dy$ Measurement

Figure 9 shows the dielectron rapidity distributions of the data after all selection. We measure the $d\sigma/dy$ distribution of the dielectron pairs using:

$$\frac{d\sigma(\gamma^*/Z)}{dy}(y) = \frac{N_{sig}(y) - N_{bkg}(y)}{\Sigma_i A \times \epsilon(y) \cdot \epsilon^i_{trig}(y) \cdot \epsilon_{zvtx} \cdot \int Ldt} \tag{2}$$

where $N_{sig}(y) - N_{bkg}(y)$ is the number of the background-subtracted events, $A \times \epsilon(y)$ is the combined acceptance and efficiency (Figure 5), and the $\epsilon^i_{trig}(y)$ is the trigger efficiency of each topology (Figure 3), the $\epsilon_{zvtx} = 95.8 \pm 0.2\%$ for $run < 212134$ and $96.8 \pm 0.2\%$ for $run \geq 212134$ is the acceptance for the $p\bar{p}$ collision vertex to occur in the central 60 cm of the detector, and $\int Ldt$ is the total integrated luminosity.

The $d\sigma(\gamma^*/Z)/dy$ measurement is shown in Figure 10 separatelly for the positive and negative rapidity. The total cross section from integrating $d\sigma(\gamma^*/Z)/dy$ is $\sigma = 258.21 \pm 0.67(statistic) \pm 4.77(systematic)$ pb. The luminosity error of 6% is not included in the systematic error of the total cross section measurement. Since the measured $d\sigma/dy$ is symmetric about y=0, we combine the results and this is shown in Figure 11.

We compare the data to three different theory predictions. The perturbative calculation is an NLO and NNLO QCD calculation. Three different PDFs are used: CTEQ6.1M, MRST2001E, and MRST2006E [3, 4, 5]. The total predicted cross section is normalized to the measured cross section, 258.21 pb. Figure 12 shows the data to theory ratios. It shows a good agreement between data and predictions and is most consistent with NLO calculation with NLO CTEQ6.1 PDF.

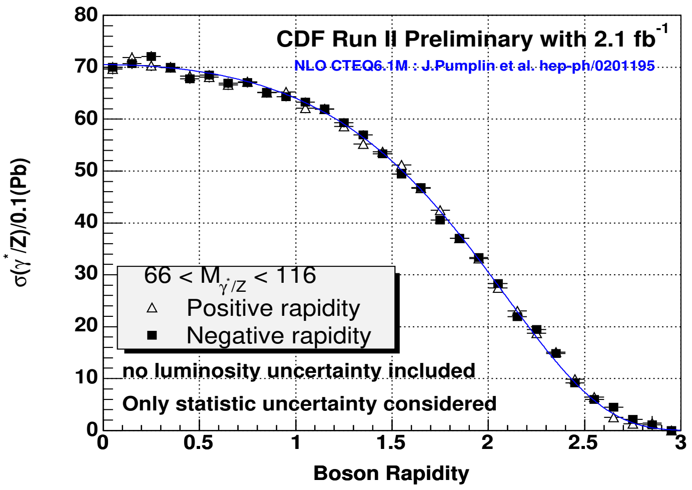

Figure 10: The measured $d\sigma/dy$ for $p\bar{p} \to Z^0/\gamma^* \to e^+e^-$ in the negative and positive rapidity. Negative rapidity directions are folded over onto positive rapidities. Only statistic uncertainties are considered.

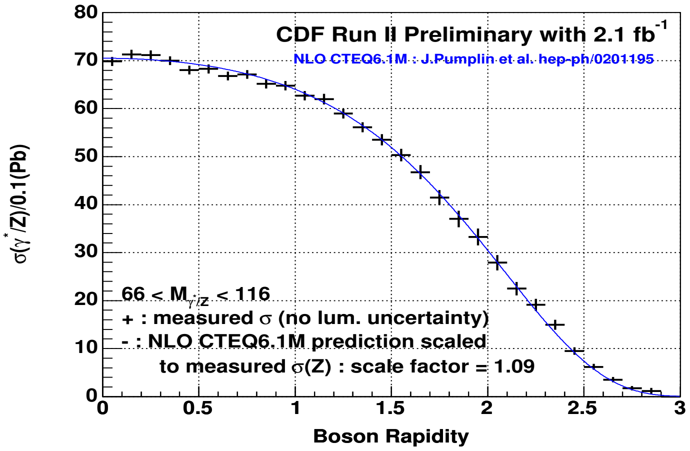

Figure 11: The measured $d\sigma/dy$ for $p\bar{p} \to Z^0/\gamma^* \to e^+e^-$. The crosses are the measurement and the solid line is the theory prediction. The prediction is the NLO calculation with NLO CTEQ6.1 PDFs. The total predicted cross section is normalized to the measured σ, $258.21 pb$. The combined uncertainties of statistic and systematic uncertainties are considered.

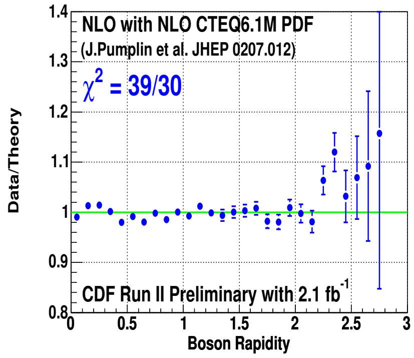

(a)

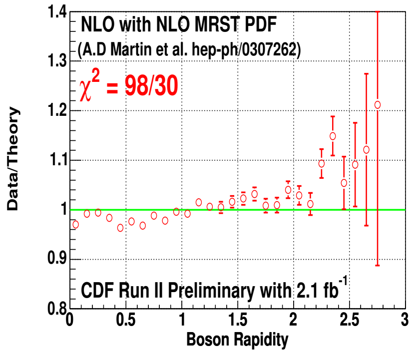

(b)

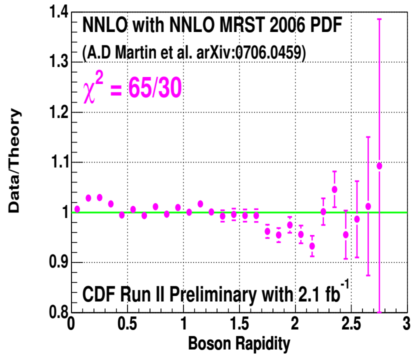

(c)

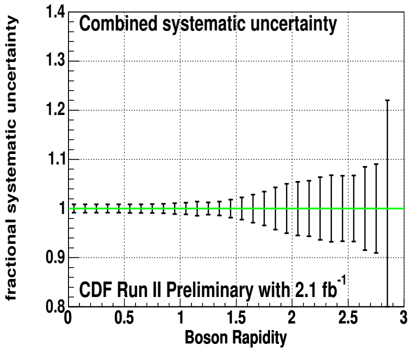

(d)

Figure 12: The ratio of the data to the theory prediction for $d\sigma/dy$. Plot (a) uses NLO calculation with NLO CTEQ6.1M PDFs, (b) uses NLO calculation with NLO MRST2001E PDFs, and (c) uses NNLO calculation with NNLO MRST2006E PDFs for the theory prediction. Only statistic uncertainties are considered for plots and chi^2 calculations. Plot (d) shows the fractional systematic uncertainty. The normalization factors for each theory predictions are 1.09(CTEQ6.1M), 1.07(MRST2001E), and 0.93(MRST2006E).

8 Conclusion

We have measured the $d\sigma/dy$ differential cross section for $p\bar{p} \to Z^0/\gamma^* \to e^+e^-$. The total cross section integrated over all dielectron rapidities is $\sigma = 258.21 \pm 0.67(statistic) \pm 4.77(systematic)$ pb. The main goal of the analysis is to compare the shape between data and theory predictions and future input to PDF fits. We find the NLO calculation with NLO CTEQ6.1 PDF to be most consistent with the data.

References

[1] CDF collaboration: T. Affolder, et al., Phys.Rev. D63 (2001), hep-ex/0006025 "Measurement of Rapidity Distribution for High Mass Drell-Yan ee Pairs at CDF"

[2] http://www-cdf.fnal.gov/physics/ewk/2006/dszdy/

[3] J. Pumplin, D.R. Stump, J. Huston, H.L. Lal, P.Nadolsky, W.K. Tung, JHEP 0207 (2002) 012, hep-ph/0201195 "New Generation of Parton Distributions with Uncertainties from Global QCD Analysis"

[4] A.D. Martin, R.G. Roberts, W.J. Stirling, and R.S.Thorne, Eur.Phys.J. C28 (2003), hep-ph/0307262 "Uncertainties of predictions from parton distributions. I: experimental errors"

[5] A.D. Martin, W.J. Stirling, R.S. Thorne and G. Watt, arXiv:0706.0459 [hep-ph] "Update of Parton Distribution at NNLO"